Article

Enhanced Electrochemical Performance of MnCo$_{1.5}$Fe$_{0.5}$O$_4$ Spinel for Oxygen Evolution Reaction through Heat Treatment

Krystian Lankauf,* Bartłomiej Lemieszek, Karolina Górnicka, Patryk Błaszczak, Marcin Zając, Piotr Jasiński, and Sebastian Molin

Cite This: https://doi.org/10.1021/acs.energyfuels.3c02875

Read Online

ACCESS | Metrics & More | Article Recommendations | SI Supporting Information

ABSTRACT: MnCo$_{1.5}$Fe$_{0.5}$O$_4$ spinel oxide was synthesized using the sol−gel technique, followed by heat treatment at various temperatures (400, 600, 800, and 1000 °C). The prepared materials were examined as anode electrocatalysts for water-splitting systems in alkaline environments. Solid-state characterization methods, such as powder X-ray diffraction and X-ray absorption spectroscopy (XAS), were used to analyze the materials' crystallographic structure and surface characteristics. The intrinsic activity of the MnCo$_{1.5}$Fe$_{0.5}$O$_4$ was fine-tuned by altering the electronic structure by controlling the calcination temperature, and the highest activity was observed for the sample treated at 800 °C. A shift in the valence state of surface cations under oxidative conditions in an alkaline solution during the oxygen evolution reaction was detected through ex situ XAS measurements. Moreover, the influence of the experimental conditions on the electrocatalytic performance of the material, including the pH of the electrolyte and the temperature, was demonstrated.
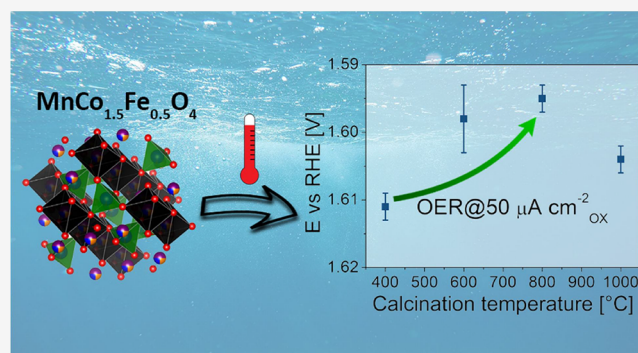
1. INTRODUCTION

MnCo$_2$O$_4$ spinel oxide is a material of interest in several applications, for example, as an anode material for water-splitting systems,[1] a protective coating for solid oxide fuel cells' interconnects,[2−4] supercapacitors,[5,6] solid oxide electrolysis cells' electrodes,[7] and lithium-ion and lithium−oxygen batteries.[8,9] Generally, MnCo$_2$O$_4$ is considered an inverse spinel with the Mn cations occupying the octahedral sites; however, depending on the preparation method and calcination temperature, a complex spinel structure may occur as Co^{2+}[Co^{2+}Mn^{4+}]O$_4$, Co^{3+}[Mn^{2+}Co^{3+}]O$_4$, Co^{2+}[Mn$^{3+}_x$Co$^{3+}_{2-x}$]O$_4$, or Co$^{2+}_{0.965}$Mn$^{2+}_{0.035}$[Mn$^{3+}_{0.78}$Mn$^{4+}_{0.21}$Co$^{2+}_{0.21}$Co$^{III}_{0.8}$].[10,11] The spinel crystallizes in a cubic structure with the space group $Fd\bar{3}m$ (no. 227). The spinel unit cell comprises 8 face-centered cubic (FCC) cells, where oxide anions occupy 32 FCC lattice points and metal cations occupy 8 tetrahedral and 16 octahedral voids.

Among the numerous materials proposed for electrocatalytic reactions, the spinel family has garnered significant interest due to the vast array of constituent elements, offering extensive tunability of the properties. For instance, Wang et al. investigated the composition effect of ZnMn$_x$Co$_{2-x}$O$_4$ (x = 0−2.0) spinel oxides on CO oxidation,[12] utilizing the local chemistry and valency characterizations of the cations. The authors suggested that Mn cations are the primary species affecting the spinel's ability to oxidize CO. The key to achieving high activity lies in the coexistence of Mn^{4+} and Mn^{3+} cations, with a ratio slightly above 1 (Mn^{4+}:Mn^{3+} ratio of 1.58). The moderate oxygen adsorption strength facilitates O vacancy refilling, which is a rate-determining step during CO oxidation.

In our recent work, Mn$_x$Co$_{3-x}$O$_4$ (x = 0, 0.5, 1, 1.5, and 2) spinel powders, fabricated via a facile EDTA-CA-EG method, were evaluated as oxygen evolution reaction (OER) electrocatalysts.[1] The findings revealed that the addition of Mn ($x \leq$ 1) to the cubic Co$_3$O$_4$ phase results in an enhanced electrocatalytic performance. The lowest overpotential was achieved for the sample designated as MnCo$_2$O$_4$, exhibiting a dual-phase structure (∼30% Co$_3$O$_4$ and ∼70% Mn$_{1.4}$Co$_{1.6}$O$_4$). A comparatively low overpotential of 327 mV was used to achieve the benchmark current density of 10 mA cm^{-2}. In another study, Chowdhury et al. investigated Ni−Co spinel oxides with varying Ni:Co ratios to examine the influence of compositional variation on the electrocatalytic activity.[13] Among the synthesized catalysts, Ni−Co oxide with a Ni:Co ratio of 1:3 demonstrated the best electrochemical perform-

A

ance, with onset potentials of 1.51 V vs RHE for the OER. The authors concluded that the enhanced electrocatalytic activity was primarily attributed to improved electronic communication through Co^{3+}/Co^{2+} and Ni^{3+}/Ni^{2+} redox couples, and a high ECSA providing ample accessible active sites. Recently, we have further improved the OER activity of $MnCo_2O_4$ by partially substituting Co with Fe.[14] When compared to pristine $MnCo_2O_4$, an ideal amount of Fe incorporated into the octahedral sites ($MnCo_{1.5}Fe_{0.5}O_4$) improved the overpotential of the OER by 30 mV (at a benchmark 10 mA cm^{-2} GEO current density). A volcano-type shape function of the e_g occupancy at octahedra sites and the OER-specific activity was observed.

Spinel oxides provide tunability of their properties through alterations to the synthesis conditions.[15−17] Magalhães et al. studied the impact of heat treatment on the catalytic properties of iron cobaltite ($FeCo_2O_4$) nanoparticles prepared via coprecipitation.[18] The XPS results revealed a higher cobalt content on the surface of nonheated samples compared to those treated to 900 °C, which was attributed to the enhanced catalytic activity in the unannealed samples. Qi et al. prepared $FeMn_2O_4$ spinel nanoparticles using coprecipitation and postannealing at varying temperatures, allowing modulation of the cationic oxidation states and optimization of the OER performance.[19] Increasing the postannealing temperature led to the changes in the spinel internal structure, with higher Fe^{2+}/Fe^{3+} and slightly increased Mn^{3+}/Mn^{2+} ratios, which were favorable for the OER performance. Under alkaline conditions, the material produced at 500 °C exhibited the best OER activity. Wei et al. prepared a series of $MnCo_2O_4$ cubic spinels by a solid-sate chemistry method at various temperatures.[20] They have observed that the Mn valence state ranges from +3.2 to +3.7, while Co does not change and remains at ∼+2.5. The authors concluded that the OER activity of various $MnCo_2O_4$ exhibits a volcano shape as a function of the Mn valence state in octahedral sites, which depends on the materials preparation temperature.

In this study, $MnCo_{1.5}Fe_{0.5}O_4$ spinel oxide (MCF500) was synthesized using the sol−gel method and subjected to heat treatment at various temperatures (400, 600, 800, and 1000 °C) to alter the valence of the constituent cations. The research focused on examining the effects of these changes on the material's physicochemical and electrochemical properties, particularly its OER electrocatalytic activity in alkaline electrolytes.

2. EXPERIMENTAL SECTION

2.1. Materials Synthesis. $MnCo_{1.5}Fe_{0.5}O_4$ spinel oxide powders were prepared using the EDTA-citric acid method described in detail in previous work.[14] The obtained powders were heat-treated at various temperatures (400, 600, 800, and 1000 °C) for 2 h in air on alumina trays. Using yttria-stabilized zirconia (YSZ, Inframat) spherical grinding media (1 mm), the calcined powders were ball-milled in ethanol for 144 h in 20 mm diameter glass vials with a rotation speed of 100 rpm to improve the electrocatalytic performance.

2.2. Characterization. With CuK radiation (= 1.5404) and a Lynxeye XE-T detector in the range of 5 to 110° with a 0.01° step size, powder X-ray diffraction (pXRD) was carried out at room temperature on a Bruker D2 Phaser diffractometer. The mean crystallite size was calculated using the Scherrer equation:

$$\tau = \frac{K\lambda}{\beta\cos\theta} \tag{1}$$

where τ is the mean size of the crystallites, K is a dimensionless shape factor (K = 0.9), λ is the X-ray wavelength, β is the line broadening at half the maximum intensity (fwhm), and θ is the Bragg angle.

The $MnCo_{1.5}Fe_{0.5}O_4$ samples were subjected to X-ray absorption spectroscopy (XAS) observations for the L2,3-edge spectra of Mn, Co, and Fe at the SOLARIS National Synchrotron Radiation Centre's 04BM PIRX (formerly PEEM/XAS) beamline.[21] A 1.31 T bending magnet is used by the PIRX beamline to deliver a photon energy range of 100 to 2000 eV with a maximum energy resolution of 2.510^{-4}. The size of the beam spot illuminating the sample was 50 μm × 40 μm (horizontal × vertical). Powder samples were placed on the carbon tape and mounted on the Omicron-type plate sample holder. The total electron yield detection mode (TEY), which reflects an information depth of several nm, was used to record the XANES spectra. Data was collected at room temperature and in UHV. The Bessy program was used to process the obtained data. The data were first adjusted to the actual incident photon flux I_0. To further analyze the data, a straight line fitted to the L_3 pre-edge region was subtracted, a polynomial function (degree 0) fitted to the L_2 postedge region was divided, and the intensity was normalized to a maximum of 1.

According to the BET isotherm model, the N2 adsorption technique (Quantachrome, NovaTouch LX1) was used to quantify the specific surface area of the powders. Prior to the sorption test, the samples were degassed for 3 h at 300 °C in a vacuum.

2.3. Electrode Preparation and Electrochemical Measurements. The powder catalysts were placed on glassy carbon rotating disc electrodes (RDE-GCE, 0.196 cm^2, ALS Co., Ltd.). The RDE GCE was polished for 5 min with 9, 3, and 1 μm polishing diamond solutions prior to the deposition of the catalyst inks. After being sonicated for 10 min in deionized water or isopropanol, it was dried overnight at room temperature. Using 1 mm YSZ grinding balls, the catalyst and Super P Li Conductive Carbon Black (CCB) (Imerys Graphite & Carbon) powder was ball-milled in ethanol for 144 h in the same manner as catalyst powders. In the proper proportion, dried spinel powder, CCB, and 5 wt % Nafion 117 solution (Sigma-Aldrich) were combined to create 1 mL of ink with a solids weight ratio of 5:5:2 (catalyst:CCB:Nafion). The inks were then sonicated for 30 min in an ice−water bath. The RDE-GCE was then drop-cast with 5 μL of the ink while it was rotating at 500 rpm, resulting in a catalyst total mass loading of 45.5 μg. In a specially constructed, three-electrode Teflon cell system with a water jacket, all electrochemical experiments were carried out in 0.1 M KOH aqueous solution (produced from 1 M KOH Titripur from Merck, diluted with DI water ∼12 MΩ). As the working (WE), counter (CE), and reference (RE) electrodes, a catalyst-coated RDE-GCE, a Pt coil, and Hg/HgO in 0.1 M KOH solution (ALS Co., Ltd., Japan) were used, respectively. The rotating disc electrode (RDE) system (RRDE-3A Rotating Ring Disc Electrode Apparatus ver. 2.0, ALS Co., Ltd.) was used in the electrochemical testing along with a BP-300 (BioLogic) bipotentiostat. To maintain the equilibrium of the O_2/H_2O over the electrolyte, a gas flow of 50 mL min^{-1} was maintained over the electrolyte for 30 min before each experiment using a 99.995% O_2 purge. A Julabo F12 thermostat was used to maintain a 25 °C electrolyte temperature. The same procedure was used for all electrocatalytic tests. Through experimental calibration of the Hg/HgO reference electrode against RHE, all recorded potentials were converted to RHE. The range of (−928: −920) mV was found to correspond to the value of E_{Offset} versus RHE, which is equivalent to the measured equilibrium potential of hydrogen electrocatalysis (HER/HOR). Ten voltage cycles in the range of 1.0−1.7 V versus RHE at a scan rate of 100 mV s were used to condition the disc electrode. The background correction for the OER polarization curves was carried out by averaging the positive- and negative-going scans. To remove the resistance of the solution, all potential values were iR-corrected. Electrochemical impedance spectroscopy in the frequency range of 10 kHz to 0.1 Hz at 0 V versus OCV with an amplitude of 10 mV and a rotation speed of 1600 rpm was used to compute the uncompensated resistance (R_u). Using the EC-Lab software, the Randles equivalent circuit was fitted. The geometric surface area of the RDE-GCE (0.196 cm^2) was used to normalize the current density
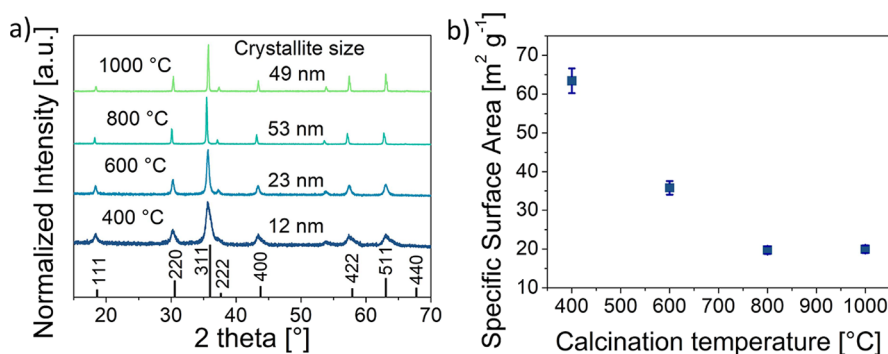
Figure 1. (a) pXRD patterns of $MnCo_{1.5}Fe_{0.5}O_4$ powders calcined at different temperatures; the XRD pattern at the bottom corresponds to reference $MnCo_2O_4$ (COD ID 2300280, $Fd\bar{3}m$, no. 227);[22] (b) specific surface area determined by BET measurements.
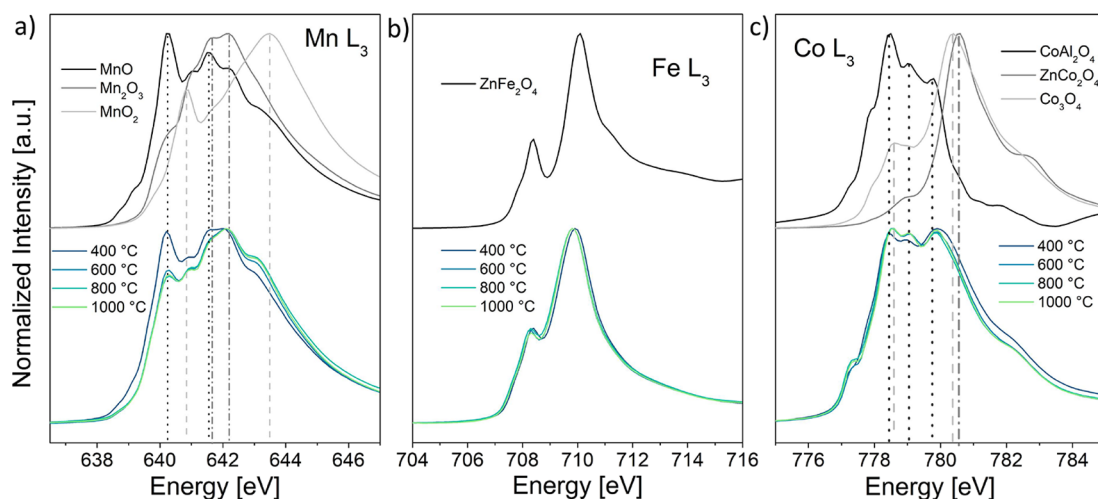

Figure 2. (a) Mn L_3, (b) Fe L_3, and (c) Co L_3 XANES spectra of $MnCo_{1.5}Fe_{0.5}O_4$ powders and several reference materials.

(expressed in the unit mA cm$^{-2}_{GEO}$). The difference between the potential at 10 mA cm$^{-2}_{GEO}$ and the typical potential of oxygen electrocatalysis (1.23 V) was used to compute the OER overpotential. Current normalization using the BET specific surface area of each oxide catalyst was used to calculate the specific (expressed in the unit μA cm$^{-2}_{OX}$). At least three different samples of each substance were made and tested for repeatability.

For the ex situ XAS measurements, 25 μL of the catalyst containing ink was deposited onto the Sigracet 39 AA carbon paper covering a surface area of 5 × 10 mm (presented in Figure S1). The electrode was subjected to OER conditions by performing the following OER protocol: 1, conditioning (10 cycles, 10 mV s^{-1}, 1–1.7 V vs RHE); 2, OER polarization (3 cycles, 10 mV s^{-1}, 1–1.9 V vs RHE); 3, chronopotentiometry (10 mA cm$^{-2}_{GEO}$, 1 h). Data collected during this protocol are presented in Figure S2. Subsequently, the electrode was dried and the XAS spectra of the Mn, Fe, and Co were collected at the PIRX beamline.

The OER tests at various temperatures were performed using a Julabo F12 thermostat to control the temperature inside the electrochemical cell (25, 31, 33, 37.5, 43.5, and 50 °C). From the experimental OER current-polarization curves, the values of a current at 0 V overpotential i_0 were extracted and used to construct Arrhenius plots. The following equation was used to calculate the apparent activation energy E_a:

$$\frac{d\ln(i_0)}{d(1/T)} = -\frac{E_a}{R} \tag{2}$$

where T is the temperature and R is the gas constant.

The influence of the pH on the OER activity was tested in the electrolytes of the following concentrations: 0.01, 0.1, and 1.0 M KOH. The exact value of the pH was measured with the CP-401 pH-

meter (Elmetron) coupled with ERH-11 combination pH electrode (Hydromet). Prior to the experiment, the pH-meter was calibrated in five buffer solutions (pH = 2, 4, 7, 9, and 12, Chempur).

3. RESULTS AND DISCUSSION

A series of $MnCo_{1.5}Fe_{0.5}O_4$ spinel oxides were synthesized using the sol−gel method, followed by calcination at various temperatures. As depicted in Figure 1, the samples used in this study were phase-pure and well-crystallized in a cubic structure (space group $Fd\bar{3}m$, no. 227). The peaks in the X-ray diffraction patterns became progressively narrower as the calcination temperature increased, indicating the growth of powder particles. According to the Scherrer equation, the crystallite diameter increased 4-fold when the calcination temperature was raised from 400 to 800 °C. Furthermore, the growth of the powder particles was corroborated by the decrease in the specific surface area, as determined by Brunauer−Emmett−Teller (BET) measurements, from 64, 36, 20, to 20 m^2 g^{-1}.

X-ray absorption near-edge spectroscopy (XANES) data for the L_3 edges were collected to investigate the valence of Mn, Co, and Fe in the prepared spinel oxides (Figure 2). Additionally, reference samples with stable and specified valence states of their constituent transition metal cations were compared (Co^{2+} in $CoAl_2O_4$, Co^{3+} in $ZnCo_2O_4$, Co^{2+} and Co^{3+} in Co_3O_4, Fe^{3+} in $ZnFe_2O_4$, Mn^{2+} in MnO, Mn^{3+} in Mn_2O_3, and Mn^{4+} in MnO_2). Since the measurements in the total electron yield mode (TEY) are surface-sensitive (nano-
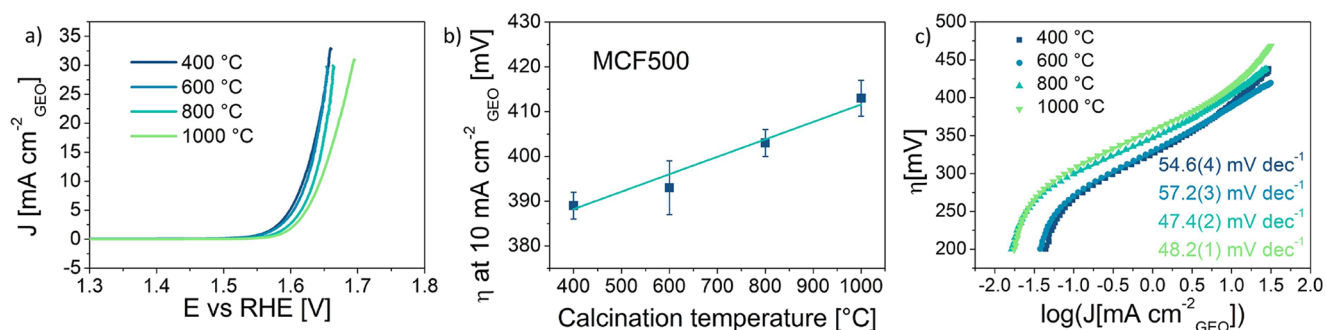
Figure 3. (a) Oxygen evolution polarization curves, corresponding (b) overpotentials η, and (c) Tafel slopes of $MnCo_{1.5}Fe_{0.5}O_4$ catalysts prepared at various temperatures.
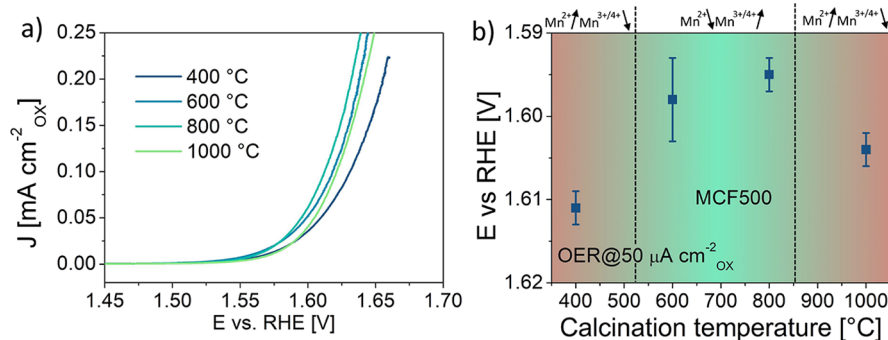

Figure 4. (a) Oxygen evolution polarization curves with current normalized by the BET specific surface area; (b) correlation between OER potentials at 50 μA cm^{-2}_{OX} and calcination temperature of $MnCo_{1.5}Fe_{0.5}O_4$ powders.
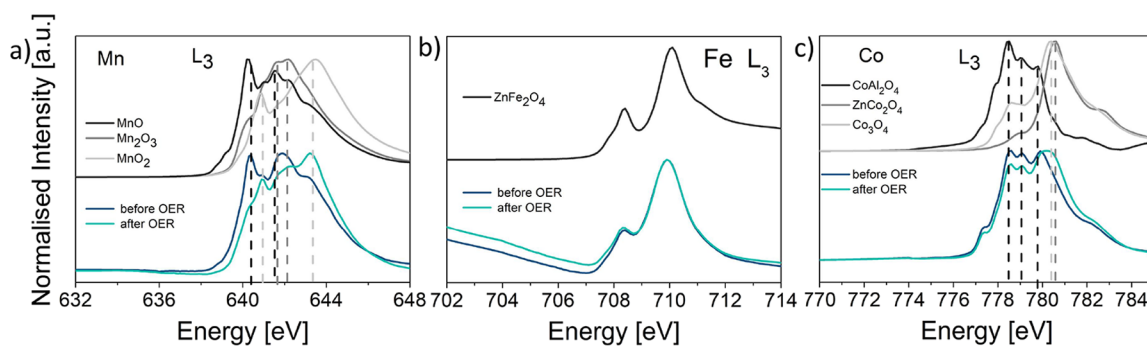

Figure 5. (a) Mn L_3, (b) Fe L_3, and (c) Co L_3 XANES spectra of $MnCo_{1.5}Fe_{0.5}O_4$ calcined at 800 °C before and after the OER testing protocol.

meter depth), the obtained results describe the valence state of surface cations.[23]

The Mn spectrum of the sample prepared at 400 °C overlaps with that of a mixture of MnO and Mn_2O_3 phases. For powder calcined at 400 °C, the relative Mn^{2+} concentration is higher than that for the powders processed at higher temperatures. The average Mn oxidation state increases with increasing processing temperature. For the powder annealed at 1000 °C, a slight shift, within the experimental error, indicating a possible lower average Mn oxidation state can be noticed at the right shoulder. As presented in Figure 2b, neither heat treatment had an impact on the Fe oxidation state. According to the Co L_3 edge spectra, all the samples exhibit a Co^{2+}/Co^{3+} ratio close to 1; however, the sample annealed at 400 °C shows a slightly lower amount of Co^{2+} (in a tetrahedral position) vs $Co^{3+/4+}$.

After low-temperature preparation at 400 °C, the sample contains more Mn in the tetrahedral position at the +2 oxidation state, whereas higher processing temperatures shift

Mn to the octahedral position. The increase of $Mn^{3+/4+}$ at octahedral positions increases the concentration of active sites as well as polaron charge carriers, influencing the electrical conductivity and electrocatalytic performance.[24,25]

The OER electrocatalytic activity of the prepared materials was tested in an alkaline environment (0.1 M KOH). As shown in Figure 3a, all the samples exhibit an onset reaction potential above 1.5 V vs RHE. To better illustrate the differences between the specific samples, the overpotentials (η) required to achieve a geometric current density of 10 mA cm^{-2} are presented in Figure 3b. The overpotentials increase linearly with the calcination temperature, ranging from approximately 390 to 415 mV. The Tafel slopes of the reported samples fall within the range of 40−60 mV dec^{-1}, suggesting that the number of electrons transferred in the rate-determining step is between 3 and 4. These values align with the evolution of O_2 through the simultaneous oxidation and formation of hydroxide and oxyhydroxide during OER.[26] The sample prepared at 800 °C exhibits the lowest Tafel slope, indicating
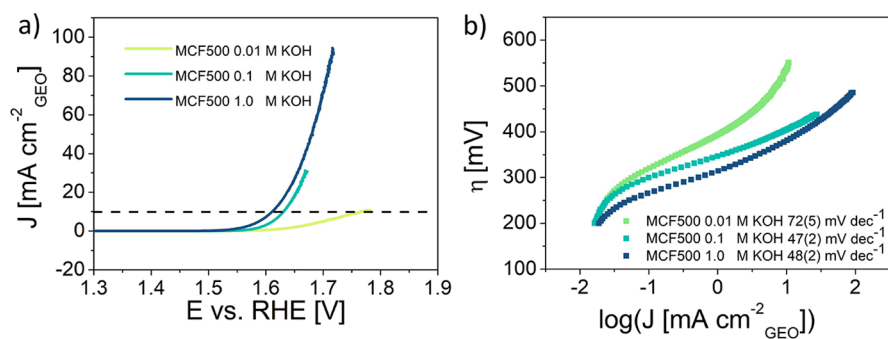
Figure 6. OER polarization curves of MnCo$_{1.5}$Fe$_{0.5}$O$_4$ 800 °C scanned in (a) different KOH solutions (12.15−14.15 pH) and (b) corresponding Tafel slopes.

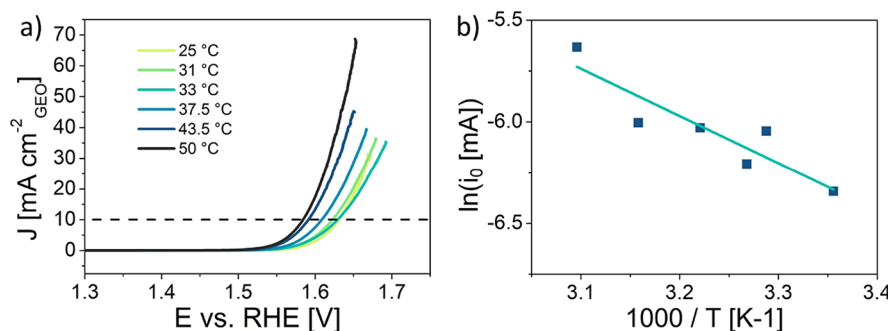**Figure 7.** OER polarization curves of MnCo$_{1.5}$Fe$_{0.5}$O$_4$ 800 °C scanned in (a) 0.1 M KOH in different temperatures and (b) corresponding Arrhenius plot.

the fastest reaction kinetics among the tested materials due to a higher number of active sites.

To gain a better understanding of the intrinsic electrocatalytic properties of the materials, the measured polarization curves were normalized using the specific surface area values obtained from the BET, as shown in Figure 4a. Due to the broad particle size distribution, which is reflected by BET surface area values ranging from 20 to 64 m^2 g^{-1}, the observed trend differs significantly from that of the polarization curves normalized with respect to the geometrical surface area. As depicted in Figure 4b, the sample calcined at 800 °C is characterized by the lowest overpotential required to sustain a current density of 50 μA cm$^{-2}_{OX}$. This aligns with previous observations including the shift to a lower Tafel value, substantiated by a higher availability of active sites, in accordance with the XANES results.

To examine the influence of oxidative conditions in the alkaline solution, ex situ XAS measurements were performed on a carbon paper electrode coated with a MnCo$_{1.5}$Fe$_{0.5}$O$_4$ 800 °C catalyst. As shown in Figure 5, the spectra of Mn and Co changed significantly, while the Fe spectrum after the OER protocol was barely affected in the background pre-edge region. After the OER protocol, the Mn spectrum shape is altered in a manner that closely aligns with the MnO$_2$ spectrum, with a small contribution from the Mn$_2$O$_3$ spectrum. This indicates a valence shift from Mn$^{2+/3+}$ to Mn$^{3+/4+}$ for surface cations. Similarly, Bergmann et al. observed a shift of the edge position in the XANES spectra corresponding to an increase of the mean Mn oxidation state to almost +4.0 of the MnO$_x$ after applying oxidative potential in 0.1 M KPi.[27] The optimal Mn valence for the OER on various Mn oxides ranges from Mn$^{3.6+}$ to Mn$^{3.8+}$.[28] A similar shift toward a higher oxidation state is observed for the Co cations. As depicted in

Figure 5c, after the OER, there is a change in the high-/low-energy peak ratio, illustrating the transition of Co cations with an oxidation state from Co^{2+} > Co^{3+} to Co^{2+} < Co^{3+}. According to Calvillo et al., the increase of Co(III) species in octahedral sites is in agreement with the formation of CoOOH in Co−Fe spinels under oxidative conditions.[29] The CoOOH is identified as the catalytic OER phase. Overall, based on the XAS results, after the OER test, the surface Mn^{2+} oxidizes to the $^{+3/+4}$ state, and the Co^{2+} oxidizes toward Co^{3+}, indicating the formation of the active sites based on Mn and Co, while Fe remains inactive.

3.1. Influence of pH and Temperature on Activity. The OER activity of the MnCo$_{1.5}$Fe$_{0.5}$O$_4$ calcined at 800 °C was tested in electrolytes with varying concentrations (0.01 M, pH = 12.15, 0.1 M, pH = 13.15, 1 M, pH = 14.15). The strong influence of the pH on the electrochemical performance is evident in Figure 6a, with the highest performance obtained in the 1 M KOH electrolyte.

The pH-dependent electrocatalyst performance suggests the presence of decoupled proton−electron transfer during the catalytic reaction.[30] A decrease in the Tafel slopes is also observed (Figure 6b). This change in the Tafel slope indicates a variation in the number of electrons transferred in the rate-determining step.[26]

Following the study of the influence of the pH, the performance of the OER was tested at various electrolyte temperatures. As illustrated in Figure 7a, a noticeable increase in activity occurs with the rising temperature. Based on the slope of the Arrhenius plot shown in Figure 7b, the apparent activation energy was calculated according to eq 1, presented in the 2. A value of 20 kJ mol^{-1} is slightly lower than the 25 kJ mol^{-1} reported for NiFeO$_x$ by Nurlaela et al.,[31] yet significantly

lower than the 71 kJ mol^{-1} for NiCoO$_x$[32] and 75 kJ mol^{-1} for Ni.[33]

The enhanced OER electrocatalysis with increasing electrolyte temperature could be attributed to accelerated kinetics and temperature-induced variations in active species. As demonstrated by Zhou et al., the active species of NiCo$_2$O$_4$ nanorod arrays at room temperature is NiCo$_2$O$_4$; however, under elevated temperature conditions, the active species transitions from NiCo$_2$O$_4$ to oxyhydroxides.[34] Moreover, NiOOH exhibits a lower overpotential compared to NiCo$_2$O$_4$.

4. CONCLUSIONS

In conclusion, this study successfully synthesized MnCo$_{1.5}$Fe$_{0.5}$O$_4$ spinel oxide using the sol−gel technique, followed by heat treatment at various temperatures. The structural properties were investigated through the XRD and XAS techniques. It was found that the preparation conditions significantly impacted the material's specific surface area and valence states, which directly influenced the electrocatalytic performance. The powder annealing temperature could be correlated with the number of active sites (redox active species). For the powder processed at 400 °C, a higher amount of Mn^{2+} was observed. For powders processed at 600 °C and especially at 800 °C, the concentration of Mn$^{3+/4+}$ was the highest, whereas for the powder processed at 1000 °C, the average Mn oxidation state decreased again. Electrochemical studies revealed that the intrinsic activity of the MnCo$_{1.5}$Fe$_{0.5}$O$_4$ spinel could be fine-tuned by controlling the powder calcination temperature. Furthermore, the pH-dependent studies of electrocatalyst performance suggested the presence of decoupled proton−electron transfer during the catalytic reaction.

ASSOCIATED CONTENT

ⓢ Supporting Information

The Supporting Information is available free of charge at https://pubs.acs.org/doi/10.1021/acs.energyfuels.3c02875.

> Optical image of the catalyst containing ink deposited onto the Sigracet 39 AA carbon paper; polarization curves of the OER protocol performed on the Sigracet 39 AA carbon paper electrode coated with MnCo$_{1.5}$Fe$_{0.5}$O$_4$ 800 °C desired for the XAS ex situ measurements (PDF)

AUTHOR INFORMATION

Corresponding Author

Krystian Lankauf − *Advanced Materials Center, Faculty of Electronics, Telecommunications and Informatics, Gdańsk University of Technology, Gdańsk 80-233, Poland;* ⓞ orcid.org/0000-0002-9941-7337; Email: krystian.lankauf@pg.edu.pl

Authors

Bartłomiej Lemieszek − *Advanced Materials Center, Faculty of Electronics, Telecommunications and Informatics, Gdańsk University of Technology, Gdańsk 80-233, Poland*

Karolina Górnicka − *Advanced Materials Center, Faculty of Applied Physics and Mathematics, Gdańsk University of Technology, Gdańsk 80-233, Poland*

Patryk Błaszczak − *Advanced Materials Center, Faculty of Applied Physics and Mathematics, Gdańsk University of Technology, Gdańsk 80-233, Poland*

Marcin Zając − *National Synchrotron Radiation Centre Solaris, Jagiellonian University, Kraków 30-392, Poland*

Piotr Jasiński − *Advanced Materials Center, Faculty of Electronics, Telecommunications and Informatics, Gdańsk University of Technology, Gdańsk 80-233, Poland*

Sebastian Molin − *Advanced Materials Center, Faculty of Electronics, Telecommunications and Informatics, Gdańsk University of Technology, Gdańsk 80-233, Poland;* ⓞ orcid.org/0000-0002-8335-7632

Complete contact information is available at:
https://pubs.acs.org/10.1021/acs.energyfuels.3c02875

Notes

The authors declare no competing financial interest.

REFERENCES

(1) Lankauf, K.; Cysewska, K.; Karczewski, J.; Mielewczyk-Gryń, A.; Górnicka, K.; Cempura, G.; Chen, M.; Jasiński, P.; Molin, S. Mn$_x$Co$_{3-X}$O$_4$ Spinel Oxides as Efficient Oxygen Evolution Reaction Catalysts in Alkaline Media. *Int. J. Hydrogen Energy* **2020**, *45*, 14867−14879.

(2) Yoon, M. Y.; Lee, E. J.; Song, R. H.; Hwang, H. J. Preparation and Properties of a MnCo$_2$O$_4$ for Ceramic Interconnect of Solid Oxide Fuel Cell via Glycine Nitrate Process. *Met. Mater. Int.* **2011**, *17* (6), 1039−1043.

(3) Saoutieff, E.; Bertrand, G.; Zahid, M.; Gautier, L. APS Deposition of MnCo$_2$O$_4$ on Commercial Alloys K41X Used as Solid Oxide Fuel Cell Interconnect: The Importance of Post Heat-Treatment for Densification of the Protective Layer. *ECS Meet. Abstr.* **2009**, *MA2009−02* (12), 1258−1258.

(4) Molin, S.; Jasinski, P.; Mikkelsen, L.; Zhang, W.; Chen, M.; Hendriksen, P. V. Low Temperature Processed MnCo$_2$O$_4$ and MnCo$_{1.8}$Fe$_{0.2}$O$_4$ as Effective Protective Coatings for Solid Oxide Fuel Cell Interconnects at 750 °C. *J. Power Sources* **2016**, *336*, 408−418.

(5) Padmanathan, N.; Selladurai, S. Mesoporous MnCo$_2$O$_4$ Spinel Oxide Nanostructure Synthesized by Solvothermal Technique for Supercapacitor. *Ionics* **2014**, *20* (4), 479−487.

(6) Tholkappiyan, R.; Naveen, A. N.; Sumithra, S.; Vishista, K. Investigation on Spinel MnCo$_2$O$_4$ Electrode Material Prepared via Controlled and Uncontrolled Synthesis Route for Supercapacitor Application. *J. Mater. Sci.* **2015**, *50* (17), 5833−5843.

(7) Zhang, L.; Tian, Y.; Liu, Y.; Jia, L.; Yang, J.; Chi, B.; Pu, J.; Li, J. Direct Electrolysis of CO$_2$ in a Symmetrical Solid Oxide Electrolysis Cell with Spinel MnCo$_2$O$_4$ as Electrode. *ChemElectroChem.* **2019**, *6* (5), 1359−1364.

(8) Chen, C.; Liu, B.; Ru, Q.; Ma, S.; An, B.; Hou, X.; Hu, S. Fabrication of Cubic Spinel MnCo$_2$O$_4$ Nanoparticles Embedded in Graphene Sheets with Their Improved Lithium-Ion and Sodium-Ion Storage Properties. *J. Power Sources* **2016**, *326*, 252−263.

(9) Zou, L.; Cheng, J.; Jiang, Y.; Gong, Y.; Chi, B.; Pu, J.; Jian, L. Spinel MnCo$_2$O$_4$ Nanospheres as an Effective Cathode Electrocatalyst for Rechargeable Lithium-Oxygen Batteries. *RSC Adv.* **2016**, *6* (37), 31248−31255.

(10) Zhao, Q.; Yan, Z.; Chen, C.; Chen, J. Spinels: Controlled Preparation, Oxygen Reduction/Evolution Reaction Application, and Beyond. *Chem. Rev.* **2017**, *117* (15), 10121−10211.

(11) Bordeneuve, H.; Tenailleau, C.; Guillemet-Fritsch, S.; Smith, R.; Suard, E.; Rousset, A. Structural Variations and Cation Distributions in $Mn_{3-X}Co_xO_4$ ($0 \leq x \leq 3$) Dense Ceramics Using Neutron Diffraction Data. *Solid State Sci.* **2010**, *12* (3), 379−386.

(12) Wang, T.; Sun, Y.; Zhou, Y.; Sun, S.; Hu, X.; Dai, Y.; Xi, S.; Du, Y.; Yang, Y.; Xu, Z. J. Identifying Influential Parameters of Octahedrally Coordinated Cations in Spinel $ZnMn_xCo_{2-X}O_4$ Oxides for the Oxidation Reaction. *ACS Catal.* **2018**, *8* (9), 8568−8577.

(13) Roy Chowdhury, S.; Ray, A.; Chougule, S. S.; Min, J.; Jeffery, A. A.; Ko, K.; Kim, Y.; Das, S.; Jung, N. Mixed Spinel Ni-Co Oxides: An Efficient Bifunctional Oxygen Electrocatalyst for Sustainable Energy Application. *ACS Appl. Energy Mater.* **2022**, *5* (4), 4421−4430.

(14) Lankauf, K.; Górnicka, K.; Błaszczak, P.; Karczewski, J.; Ryl, J.; Cempura, G.; Zając, M.; Bik, M.; Sitarz, M.; Jasiński, P.; Molin, S. Tuning of E_g Electron Occupancy of $MnCo_2O_4$ Spinel for Oxygen Evolution Reaction by Partial Substitution of Co by Fe at Octahedral Sites. *Int. J. Hydrogen Energy* **2023**, *48* (24), 8854−8866.

(15) Baig, M. M.; Yousuf, M. A.; Agboola, P. O.; Khan, M. A.; Shakir, I.; Warsi, M. F. Optimization of Different Wet Chemical Routes and Phase Evolution Studies of $MnFe_2O_4$ Nanoparticles. *Ceram. Int.* **2019**, *45* (10), 12682−12690.

(16) Jbara, H. B.; Aubry, E.; Kanzari, M.; Billard, A.; Yazdi, M. A. P. Effect of Thermal Annealing on the Optoelectronic Properties of Cu-Fe-O Thin Films Deposited by Reactive Magnetron Co-Sputtering. *Thin Solid Films* **2021**, *721*, No. 138538.

(17) Chavarriaga, E. A.; Lopera, A. A.; Bender Wermuth, T.; Arcaro, S.; Bezzon, V. D. N.; García, C.; Alarcón, J.; Gabriel Ramirez, J.; Moreno, R.; Pérez Bergmann, C. Influence of Caffeine and Citrulline on Magnetic Properties When Used as New Fuels in the Synthesis of $CoFe_2O_4$ Nanoparticles by Gel Combustion. *J. Magn. Magn. Mater.* **2022**, *560*, No. 169632.

(18) Magalhães, R.; Bargiela, P.; da Rocha, M. D. G.; Gil, E.; de Souza, A. Iron Cobaltite ($FeCo_2O_4$) Nanocatalysts for Water-Oxidation: Effects of Annealing Temperature on Catalytic Properties. *J. Braz. Chem. Soc.* **2022**, *33* (10), 1163−1171.

(19) Qi, C.; Liu, Q.; Dong, Y.; Zhang, G.; Jiang, X.; Gao, D. Fe 3+ in a Tetrahedral Position Determined the Electrocatalytic Properties in $FeMn_2O_4$. *RSC Adv.* **2022**, *12* (42), 27206−27211.

(20) Wei, C.; Feng, Z.; Scherer, G. G.; Barber, J.; Shao-Horn, Y.; Xu, Z. J. Cations in Octahedral Sites: A Descriptor for Oxygen Electrocatalysis on Transition-Metal Spinels. *Adv. Mater.* **2017**, *29*, 1606800.

(21) Zając, M.; Giela, T.; Freindl, K.; Kollbek, K.; Korecki, J.; Madej, E.; Pitala, K.; Kozioł-Rachwał, A.; Sikora, M.; Spiridis, N.; Stępień, J.; Szkudlarek, A.; Ślęzak, M.; Ślęzak, T.; Wilgocka-Ślęzak, D. The First Experimental Results from the 04BM (PEEM/XAS) Beamline at Solaris. *Nucl. Inst. Methods Phys. Res., Sect. B* **2021**, *492*, 43−48, DOI: 10.1016/j.nimb.2020.12.024.

(22) Purwanto, A.; Fajar, A.; Mugirahardjo, H.; Fergus, J. W.; Wang, K. Cation Distribution in Spinel $(Mn,Co,Cr)_3O_4$ at Room Temperature. *J. Appl. Crystallogr.* **2010**, *43* (3), 394−400.

(23) Abbate, M.; Goedkoop, J. B.; de Groot, F. M. F.; Grioni, M.; Fuggle, J. C.; Hofmann, S.; Petersen, H.; Sacchi, M. Probing Depth of Soft X-ray Absorption Spectroscopy Measured in Total-electron-yield Mode. *Surf. Interface Anal.* **1992**, *18* (1), 65−69.

(24) Gillot, B.; Kharroubi, M.; Metz, R.; Legros, R.; Rousset, A. Electrical Properties of Copper Manganite Spinels $Cu_xMn_{3-x}O_4$ (0 > x > 1). *Phys. Status Solidi* **1991**, *124* (1), 317−325.

(25) DORRIS, S. E.; MASON, T. O. Electrical Properties and Cation Valencies in Mn_3O_4. *J. Am. Ceram. Soc.* **1988**, *71* (5), 379−385.

(26) Anantharaj, S.; Karthick, K.; Kundu, S. Evolution of Layered Double Hydroxides (LDH) as High Performance Water Oxidation Electrocatalysts: A Review with Insights on Structure, Activity and Mechanism. *Mater. Today Energy* **2017**, *6*, 1−26.

(27) Bergmann, A.; Zaharieva, I.; Dau, H.; Strasser, P. Electrochemical Water Splitting by Layered and 3D Cross-Linked Manganese Oxides: Correlating Structural Motifs and Catalytic Activity. *Energy Environ. Sci.* **2013**, *6* (9), 2745−2755.

(28) Risch, M.; Stoerzinger, K. A.; Han, B.; Regier, T. Z.; Peak, D.; Sayed, S. Y.; Wei, C.; Xu, Z.; Shao-Horn, Y. Redox Processes of Manganese Oxide in Catalyzing Oxygen Evolution and Reduction: An in Situ Soft X-Ray Absorption Spectroscopy Study. *J. Phys. Chem. C* **2017**, *121* (33), 17682−17692.

(29) Calvillo, L.; Carraro, F.; Vozniuk, O.; Celorrio, V.; Nodari, L.; Russell, A. E.; Debellis, D.; Fermin, D.; Cavani, F.; Agnoli, S.; Granozzi, G. Insights into the Durability of Co-Fe Spinel Oxygen Evolution Electrocatalysts: Via Operando Studies of the Catalyst Structure. *J. Mater. Chem. A* **2018**, *6* (16), 7034−7041.

(30) Zhou, Y.; Sun, S.; Song, J.; Xi, S.; Chen, B.; Du, Y.; Fisher, A. C.; Cheng, F.; Wang, X.; Zhang, H.; Xu, Z. J. Enlarged Co-O Covalency in Octahedral Sites Leading to Highly Efficient Spinel Oxides for Oxygen Evolution Reaction. *Adv. Mater.* **2018**, *30* (32), 1−7.

(31) Nurlaela, E.; Shinagawa, T.; Qureshi, M.; Dhawale, D. S.; Takanabe, K. Temperature Dependence of Electrocatalytic and Photocatalytic Oxygen Evolution Reaction Rates Using NiFe Oxide. *ACS Catal.* **2016**, *6* (3), 1713−1722.

(32) Davidson, C.; Kissel, G.; Srinivasan, S. Electrode Kinetics of the Oxygen Evolution Reaction at $NiCo_2O_4$ from 30% KOH. Dependence on Temperature. *J. Electroanal. Chem.* **1982**, *132* (C), 129−135.

(33) Miles, M. H.; Kissel, G.; Lu, P. W. T.; Srinivasan, S. Effect of Temperature on Electrode Kinetic Parameters for Hydrogen and Oxygen Evolution Reactions on Nickel Electrodes in Alkaline Solutions. *J. Electrochem. Soc.* **1976**, *123* (3), 332−336.

(34) Zhou, T.; Wang, C.; Shi, Y.; Liang, Y.; Yu, Y.; Zhang, B. Temperature-Regulated Reversible Transformation of Spinel-To-Oxyhydroxide Active Species for Electrocatalytic Water Oxidation. *J. Mater. Chem. A* **2020**, *8* (4), 1631−1635.